Biophysical Chemistry 245 (2019) 41–52

Contents lists available at ScienceDirect

Biophysical Chemistry

journal homepage: www.elsevier.com/locate/biophyschem

Requirements for band-pass activation of Ca^{2+}-sensitive proteins such as NFAT

Arne Schoch*, Jürgen Pahle

Center for Modelling and Simulation in the Biosciences (BIOMS), Center for Quantitative Analysis of Molecular and Cellular Biosystems (BioQuant), Heidelberg University, 69120 Heidelberg, Germany

HIGHLIGHTS

- Antagonistic, oscillator-dependent regulation enables band-pass activation of NFAT.
- Further, for band-pass activation regulators have to differ in their responsiveness.
- Cooperative activation events foster the distinctness of frequency-decoding.
- Also the parametrisation of binding constants impacts the distinctness of decoding.
- A system's speed determines the usable bandwidth for decoding.

GRAPHICAL ABSTRACT

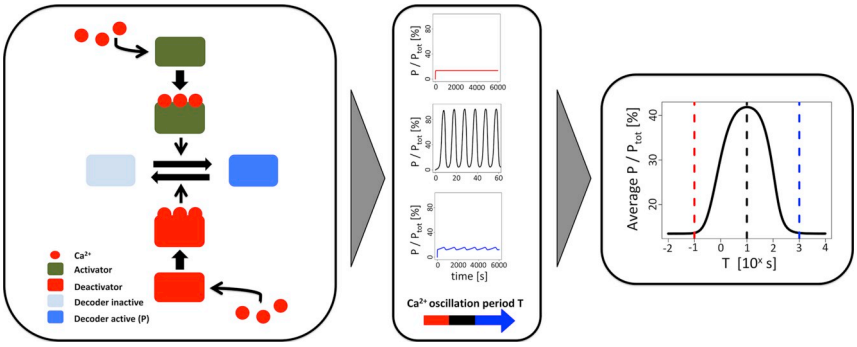

ARTICLE INFO

Keywords:
Calcium Signalling
Nuclear factor of activated T cells
Decoding
Oscillation
Frequency
Cooperativity

ABSTRACT

Several proteins are sensitive to frequency-modulated oscillations of calcium levels. Most of them exhibit increased activities for faster frequencies, a characteristic here referred to as high-pass activation. In contrast, the transcription factor NFAT is optimally activated at a specific frequency, a behaviour we call band-pass activation.

We constructed a kinetic model of NFAT activation, confirming its ability for band-pass activation at experimentally observed frequencies. To characterise the requirements for band-pass activation further, we developed a minimal model, identifying antagonistic, calcium-dependent regulation with differently responsive regulators as essential for band-pass activation. Further, in optimisations cooperative binding proved to be an important feature for distinct frequency-decoding in models of high- and band-pass activation. A subsequent analysis of the optimised parameter sets revealed the most sensitive parameters along with additional preconditions for efficient decoding.

Our analysis is not limited to NFAT, but potentially applies to any protein showing high- or band-pass activation.

1. Introduction

In many cell types, oscillations in the intracellular levels of the second messenger calcium are believed to encode information on the nature and abundance of an upstream stimulus, such as a hormone. It was observed that variations in an upstream stimulus can lead to alterations in the oscillation's amplitude, frequency, and duration [1]. Also, the waveform of the oscillation is dependent on the stimulus type.

* Corresponding author at: Im Neuenheimer Feld 267, 69120 Heidelberg, Germany.
E-mail addresses: Arne.Schoch@bioquant.uni-heidelberg.de (A. Schoch), Juergen.Pahle@bioquant.uni-heidelberg.de (J. Pahle).

https://doi.org/10.1016/j.bpc.2018.10.005
Received 16 August 2018; Received in revised form 11 October 2018; Accepted 16 October 2018
Available online 29 October 2018
0301-4622/

In hepatocytes for instance, stimulation with the hormon vasopressin results in spiking oscillations [2], while stimulation with the nucleotide adenosine triphosphate (ATP) leads to bursting oscillations characterised by a primary peak succeeded by smaller secondary ones [3]. It is known that sustained elevated levels of calcium in the cytosol can be toxic to the cell, even inducing cell death [1]. Furthermore, evidence emerged that calcium oscillations do not only prevent damaging effects, but that the encoded information on a stimulus can also be decoded by calcium-sensitive target proteins. This results in a selective activation of proteins by calcium based on specific parameters of its oscillation [4,5].

In this study, we focus on the decoding of information by dependent proteins that is encoded into the frequency of calcium oscillations. In a number of cases, proteins exhibiting activities sensitive to the frequency of calcium oscillations were observed experimentally. Among these proteins are Ca^{2+}/calmodulin-dependent protein kinase II (CaMKII) [6], protein kinase C γ [7], calpain [8] as well as the transcription factors nuclear factor kappa-light-chain-enhancer of activated B cells (NF-κB) [9] and nuclear factor of activated T cells (NFAT) [9,10]. Further, Tadross et al. showed how a sensory complex, composed of calmodulin and a calcium channel protein, decodes local and global calcium signals that differ in their signal amplitude and frequency [11]. For a more detailed review on frequency-decoders in calcium signalling, please refer to [4].

For most frequency-decoding proteins, it was found that their activities increase upon increases in the calcium oscillation frequency. We refer to this decoding mechanism as high-pass activation in the following. However, the transcription factor NFAT indicates a more complex behaviour; its activity is optimal for a particular frequency, with frequencies slower or faster only leading to a reduced activity. We call this decoding mechanism band-pass activation. A decline in NFAT activity upon increasingly slow calcium oscillations was reported for different cell types (from 10 mHz downwards in Jurkat cells [9] and from 11 mHz downwards in BHK and again Jurkat cells [12]). For faster oscillations, Li et al. found an optimum in NFAT activity in RBL-2H3 cells followed by a decrease in activity upon further increases in the oscillation frequency [10]. Also in cardiac cells increasingly fast oscillations (from 20 mHz upwards) resulted in a decrease in activity of the transcription factor [13].

It is known that NFAT activity is increased by a dephosphorylation event catalysed by calcineurin, a calcium- and calmodulin-dependent serine/threonine phosphatase, that binds to NFAT in the process. The dephosphorylated conformation of NFAT is potent of being transported to the nucleus, where it can act as a transcription factor [14]. Elevated levels of calcium, as in calcium oscillations, can elicit an accumulation of dephosphorylated NFAT by activation of calcineurin [4]. However, kinases counteract the translocation of NFAT, for instance by rephosphorylation [15,16]. Several kinases were identified that reduce NFAT activity, but for the described band-pass activation Smedler and Uhlén suggested the action of a calcium-dependent deactivator alongside the known calcium-dependent activator calcineurin [4]. In fact, experiments conducted by MacDonnel et al. and Hashimoto et al. showed that the calcium- and calmodulin-dependent serine/threonine kinase CaMKII lowers NFAT activity in neonatal rat cardiomyocytes as well as adult feline ventricular myocytes by reducing the activity of calcineurin [17–19]. In addition, downregulation of NFAT's transcriptional activity by CaMKII was reported in human T cells [20]. We hypothesise that the frequency of the calcium oscillations determines whether activating phosphatases or deactivating kinases are dominant. Therefore, their interplay enables band-pass activation of downstream NFAT. We test this hypothesis by means of an NFAT signalling model that shows optimal activation at a specific oscillation frequency. Further dissecting this behaviour, we set up a minimal model for band-pass activation, allowing us to identify requirements for efficient band-pass activation such as optimal ranges of kinetic parameters. Similarly, we search for optimal model structures and parameter margins for high-pass activation.

We would like to highlight that many calcium-dependent proteins bind calcium ions in a cooperative manner, e.g. calmodulin [21], calcineurin [22], CaMKII [23] or conventional isoforms of protein kinase C [24]. Therefore, we also investigate the effect of cooperativity on the frequency-decoding performance.

2. Methods

2.1. The cellular communication channel

In this study, we analyse the decoding of the calcium oscillation frequency by calcium-sensitive proteins. Defining a communication channel, we use the calcium oscillation period length T (the reciprocal of the frequency f) as the input of the channel. The output of the channel is the average concentration of active, calcium-dependent protein, a proxy of its average activity referred to as $\overline{P}$. A protein is capable of frequency-decoding, if its average activity significantly changes for varying values of T.

2.2. Calcium oscillations

We use simple calcium oscillation shapes as inputs for different models of protein activation. The input time series is always fixed, meaning that it cannot be altered by feedback mechanisms that might be present in the real signalling pathway.

For the stimulation of minimal models for high-pass and band-pass activation, oscillation dynamics are mimicked by a sine function with the oscillation period T as input parameter. On the basis of measurements in rat hepatocytes, trough and peak concentration of the sine wave are set to 200 nM and 1000 nM, respectively [25]. The sine wave equation for the time evolution of the calcium concentration in nM reads as follows:

$$Ca(t) = 400 \cdot \sin\left(\frac{2\pi}{T} \cdot t\right) + 600, \tag{1}$$

where period length T is the reciprocal of the oscillation frequency f.

In contrast, for the stimulation of the NFAT model, we use square wave functions. The reason for this is that square waves more closely resemble the oscillations in experiments that we refer to for parameter fitting. Here, the baseline is set to the experimentally measured concentration of 100 nM, while the peak concentration remains at 1000 nM. The active phase of the square wave is set to a fixed duration, when sampling different frequencies. This means that decreasing the frequency only increases the inactive phase.

Therefore, when we test for frequency-decoding by varying the oscillation frequency, the average oscillator concentration remains on a constant level upon changes in f in the minimal models or increases with increasing f in the NFAT model. We use the *OscillatorGenerator*, an R package, that we make publicly available on the Comprehensive R Archive Network (CRAN) at https://cran.r-project.org/package=OscillatorGenerator, for the generation of discrete, parametrisable time series of square wave oscillations.

2.3. A measure for average protein activity

The average activity $\overline{P}$ of a protein is defined as the average concentration of the active conformation P over a time period spanning from 0 s to t_{end} s:

$$\overline{P} := \frac{1}{t_{end}} \cdot \int_0^{t_{end}} [P]dt \tag{2}$$

The average activity of a species is dependent on the observed time span. Therefore, the calculation of $\overline{P}$ requires the passing of several oscillation cycles for convergence to an approximately stable level. Here, t_{end} is set to finite values that enable this convergence. In case no convergence is reached at t_{end}, the simulation results are discarded.

In the minimal models, t_{end} is set to 5000 s for sine wave inputs with T equal to 0.1 s and 10 s. For a sine wave input with T equal to 1000 s, t_{end} is selected to be 50,000 s. In the NFAT model and its variants, a uniform t_{end} of 30,000 s is chosen irrespective of the applied square wave frequency.

With respect to the minimal models, transient phases in the time course of the decoder's average activity $\overline{P}$ are shortened by initiating simulations from the steady states of the simulated species for a constant input concentration of 600 nM, which is the mean of the applied sine input oscillating between 200 nM and 1000 nM. Steady state calculations can be found in the Supplementary material.

2.4. Deterministic simulations

Deterministic simulations are run in R version 3.4.0, using the *deSolve* package [26,27]. Increased simulation speed is achieved by outsourcing the differential equations to C-code, which is then dynamically linked to R. In order to numerically integrate the ordinary differential equation systems, the LSODA solver is employed [28]. Simulations are run on a Linux (CentOS 6.4 x86 64-bit Kernel 2.6.32) compute cluster with Sun Fire AMD Opteron and IBM Quad Intel Xeon CPUs.

2.5. Optimisation of frequency-decoding

We aim at maximising the efficiency of frequency-decoding, in particular the size of changes in $\overline{P}$ upon applying different values for the period length T of the input oscillation. In high-pass activation, $\overline{P}$ is maximal for small values of T and minimal for large values of T. High-pass activation efficiency Eff_H is defined as follows (Fig. 1, panel A):

$$Eff_H := \overline{P(T_{fast})} - \overline{P(T_{slow})} \tag{3}$$

Maximisation of Eff_H over a subset of model parameters Θ yields the high-pass potential E_H:

$$E_H := \max_{\Theta} \{Eff_H(\Theta)\} \tag{4}$$

In band-pass activation, $\overline{P}$ is small at small and large values of T and maximal at an intermediate T. We define the band-pass activation efficiency Eff_B accordingly (Fig. 1, panel B):

$$Eff_B := \overline{P(T_{med})} - \overline{P(T_{ext})}, \tag{5}$$

with $\overline{P(T_{ext})}$ being the maximum of $\overline{P(T_{fast})}$ and $\overline{P(T_{slow})}$, both being smaller than $\overline{P(T_{med})}$. Maximisation of Eff_B over a subset of model parameters Θ yields the band-pass potential E_B:

$$E_B := \max_{\Theta} \{Eff_B(\Theta)\} \tag{6}$$

All optimisation runs are executed in R with the built-in *optim* function [26]. Here, the Nelder-Mead method, also known as the downhill-simplex method, is selected [29]. We employ a multi-start optimisation scheme, drawing initial parameter sets from random distributions in 500 to 50,000 runs per optimisation problem. The overall best objective value is taken as the approximated global optimum of the underlying optimisation problem. Exemplary optimisation scripts can be found in the Supplementary material.

3. Results

3.1. Antagonistic, calcium-dependent regulation allows for band-pass activation of NFAT

According to experimental results, the transcription factor NFAT exhibits band-pass activation with respect to the frequency of cytosolic calcium oscillations [4,10,13]. Smedler and Uhlén hypothesised that band-pass activation is achieved by a calcium-dependent regulation of NFAT delivered by an antagonistically acting activator-inhibitor couple [4]. A number of articles describe calcineurin as an activator of NFAT translocation to the nucleus [15,30] and therefore of NFAT's transcriptional activity. CaMKII's role as an inhibitor of NFAT in the cytosol is less well known [17,18]. Here, we present a kinetic model for NFAT activation in the cytosol that comprises CaMKII- as well as calcineurin-mediated regulation. We focused on the core mechanism of band-pass activation. Thus, our model leaves out some details that have been described in the literature. For instance, calmodulin as a common activator of calcineurin and CaMKII is not modelled explicitly [31]. Also, we neglect differences in the activity of various intermediates in CaMKII signalling [32]. Furthermore, we do not claim quantitative accuracy of our model. The aim of our model is to probe for a potential mechanism for band-pass activation in calcium-dependent NFAT activation and these simplifications help us to find the essential components in this system.

Fig. 2 gives an overview of the model, and Table 1 provides a list of reactions and the corresponding kinetic functions. In the model, inactive calcineurin, *Cn*, and Ca^{2+}/calmodulin-dependent protein kinase II, *CaMKII*, are activated by cooperative binding of calcium, *Ca*. Activated calcineurin, Cn^*, is able to form a complex, $NFAT{:}Cn^*$, which is competent for being translocated to the nucleus. NFAT is dephosphorylated in the process, but this step is not explicitly modelled. Similarly, a phosphorylated, calcium-activated calcineurin version, CnP^*, can form a competent complex, $NFAT{:}CnP^*$. However, CnP^*'s activity with respect to *NFAT* complex formation is reduced by the introduction of the inhibition factor δ. Since $CaMKII^*$ mediates the phosphorylation of *Cn*, it inhibits the generation of active complexes by forming less potent calcineurin forms. We created the structure of the model based

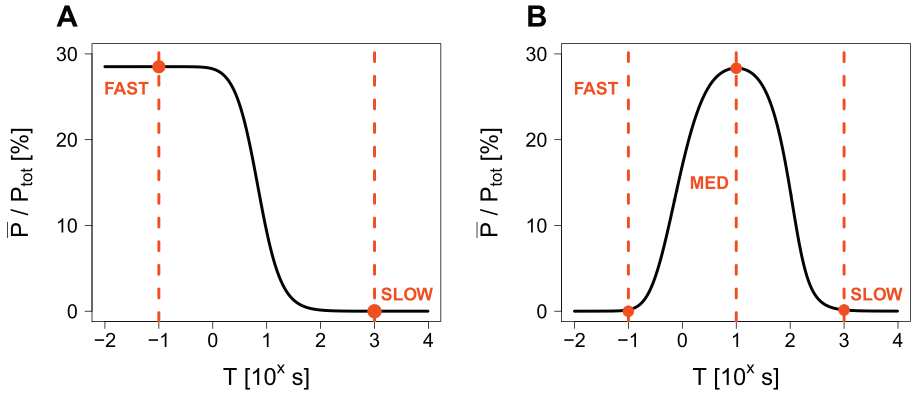

Fig. 1. Definition of high-pass and band-pass activation efficiencies. (**A**) For high-pass activation, the corresponding efficiency Eff_H is defined as the difference between $\overline{P(T_{fast})}$ and $\overline{P(T_{slow})}$. (**B**) For band-pass activation, Eff_B is defined as the difference between $\overline{P(T_{med})}$ and the maximum of $\overline{P(T_{fast})}$ and $\overline{P(T_{slow})}$. In the provided example graphs, T_{fast}, T_{med} and T_{slow} are set to the default values of 0.1 s, 10 s and 1000 s, respectively.

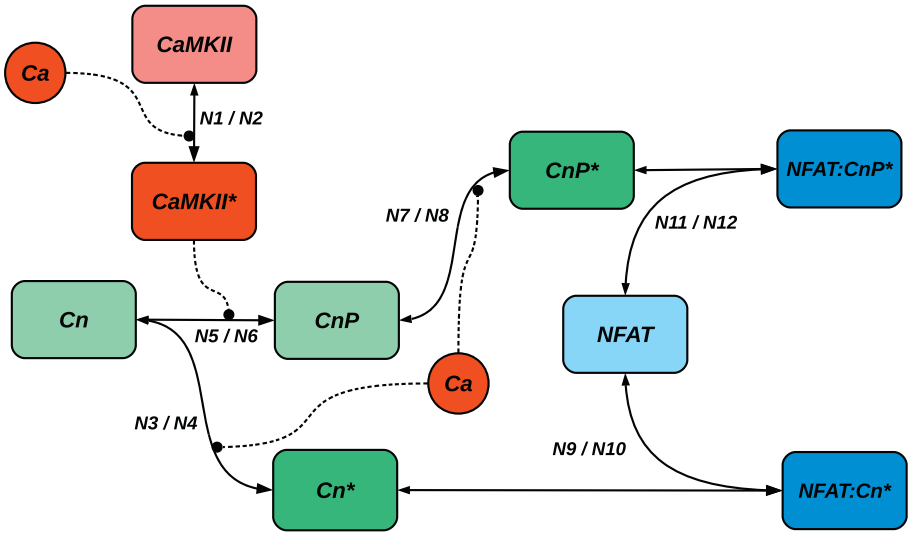

Fig. 2. Overview of the NFAT model. *CaMKII* and *Cn* are activated by *Ca*. *CaMKII** inhibits *NFAT* activation by phosphorylation of *Cn*, since *CnP** is less potent in forming an active compound with *NFAT* compared to unphosphorylated *Cn**. Round-shaped arrowheads with dashed lines refer to an activation. Reaction names refer to the kinetics presented in Table 1.

Table 1
The NFAT model's structure and kinetics. *Cn* is activated by cooperative binding of calcium, *Ca*. *Cn* can also change to a phosphorylated form, *CnP*, prior to its activation by *Ca*. Phosphorylation is carried out by calcium-bound *CaMKII**. *CnP** as well as *Cn** are able to form active complexes with *NFAT*, however, *CnP**'s activity is reduced by the introduction of δ (defined to be larger than 1).

Reactions			Kinetics
$CaMKII$	$\xrightarrow{Ca}$	$CaMKII^*$	$v_{N1} = \frac{k_{N1} \cdot CaMKII \cdot Ca^m}{K_{N1}{}^m + Ca^m}$
$CaMKII^*$	$\rightarrow$	$CaMKII$	$v_{N2} = k_{N2} \cdot CaMKII^*$
Cn	$\xrightarrow{Ca}$	Cn^*	$v_{N3} = \frac{k_{N3} \cdot Cn \cdot Ca^n}{K_{N2}{}^n + Ca^n}$
Cn^*	$\rightarrow$	Cn	$v_{N4} = k_{N4} \cdot Cn^*$
Cn	$\xrightarrow{CaMKII^*}$	CnP	$v_{N5} = k_{N5} \cdot CaMKII^* \cdot Cn$
CnP	$\rightarrow$	Cn	$v_{N6} = k_{N6} \cdot CnP$
CnP	$\xrightarrow{Ca}$	CnP^*	$v_{N7} = \frac{k_{N3} \cdot CnP \cdot Ca^n}{K_{N2}{}^n + Ca^n}$
CnP^*	$\rightarrow$	CnP	$v_{N8} = k_{N4} \cdot CnP^*$
$Cn^* + NFAT$	$\rightarrow$	$NFAT{:}Cn^*$	$v_{N9} = k_{N7} \cdot Cn^* \cdot NFAT$
$NFAT{:}Cn^*$	$\rightarrow$	$Cn^* + NFAT$	$v_{N10} = k_{N8} \cdot NFAT{:}Cn^*$
$CnP^* + NFAT$	$\rightarrow$	$NFAT{:}CnP^*$	$v_{N11} = \frac{k_{N7} \cdot CnP^* \cdot NFAT}{\delta}$
$NFAT{:}CnP^*$	$\rightarrow$	$CnP^* + NFAT$	$v_{N12} = k_{N8} \cdot NFAT{:}CnP^*$

on experimental results, stating that a phosphorylation of calcium-bound calcineurin is not possible due to allosteric constraints. Yet binding of calcium to phosphorylated calcineurin was observed [19]. We used the sum of the average activities of the two complexes *NFAT*:*Cn** and *NFAT*:*CnP** over a certain time interval as the model's output. Both forms were assumed to be equally potent:

$$\overline{NFAT^*} := \overline{NFAT{:}Cn^*} + \overline{NFAT{:}CnP^*} \tag{7}$$

In the next step, we tested whether our model is able to reproduce band-pass activation over a physiologically plausible range of frequencies, while at the same time is qualitatively agreeing with frequency-specific NFAT activity data published by Dolmetsch et al. [9]. To this end, we used an optimisation procedure as described in the Methods section. The objective function Ψ_{NFAT}, which we used for this optimisation, combines the maximisation of the band-pass efficiency Eff_B with a fit of the model behaviour to the data by Dolmetsch et al. With respect to band-pass efficiency, the period length leading to optimal activation, T_{med}, was set to 60 s based on reports in [4,10]. T_{fast} and T_{slow} were chosen to be 25 s and 500 s, respectively.

$$\Psi_{NFAT} := Eff_B(\Theta_{NFAT}) + \frac{1}{\rho}(\Theta_{NFAT}), \tag{8}$$

with $\Theta_{NFAT} = (k_{N1-8}, K_{N1-2}, m, n, \beta, \gamma, \delta)$ and ρ defined as follows:

$$\rho = (A_{data} - (A_{NFAT} \cdot \beta + \gamma))^2 + (B_{data} - (B_{NFAT} \cdot \beta + \gamma))^2 + (C_{data} - (C_{NFAT} \cdot \beta + \gamma))^2 + (D_{data} - (D_{NFAT} \cdot \beta + \gamma))^2, \tag{9}$$

where A_{data} to D_{data} are the measurements in Fig. 3b of Dolmetsch et al. [9] and A_{NFAT} to D_{NFAT} are the model's output for a comparable calcium oscillation input. All model values refer to $\overline{NFAT^*}$ relative to the total concentration of NFAT in the model in per cent. β and γ are scaling factor and offset to account for the fact that the model's output is measured in activated NFAT, whereas the experimental data refers to gene expression.

In all simulations of the model, square wave inputs were used to resemble calcium oscillations in the experiments. Parameters of the discrete square wave time series were defined as described in Table 2.

As shown in Fig. 3 panel A, our model is capable of band-pass activation at physiological frequencies. With the same optimised parameter set a resemblance to Dolmetsch et al.'s data is also present (Fig. 3 panel B). For the presented results, T_{slow} was set to 500 s. It was observed that smaller values of T_{slow} lead to faster decreasing slopes that resemble the data by Dolmetsch et al. even better, however come at the expense of a reduced band-pass activation potential (for $T_{slow} = 500$ s, $E_B = 35\%$; for $T_{slow} = 300$ s, $E_B = 31\%$; for $T_{slow} = 200$ s, $E_B = 27\%$; for the corresponding plots and optimised parameter sets please refer to the Supplementary material).

Table 2
Parameters of the applied square wave time series. Square waves were generated by means of the "SquareSpike" function in the *OscillatorGenerator* package for R. For all inputs, baseline and peak levels were set to 100 nM and 1000 nM, respectively. Parameter "trend" was fixed to 1. Column "Task" refers to the purpose of the generated input in the optimisation process. Active phase is the time span in an oscillation cycle, in which the square wave is on its peak level. Duty cycle is defined as the ratio of active phase to the oscillation period *T*.

Task	Period *T* [s]	Duty cycle [%]	Active phase [s]
Fitting to gene expression data [9]	100	10	10
	400	2.5	10
	900	1.11	10
	1800	0.56	10
Band-pass activation	25	80	20
	60	33.33	20
	500	4	20

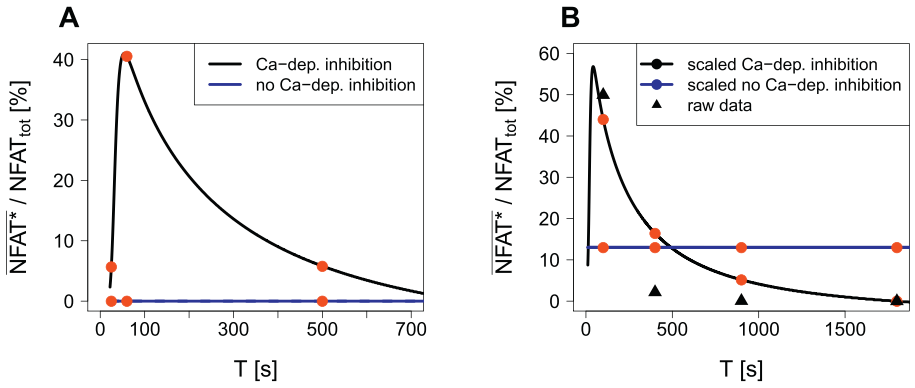

Fig. 3. Optimisation results for the NFAT model. The NFAT model was optimised according to Ψ_{NFAT} (Eq. (8)) in order to generate band-pass activation as well as to perform a qualitative fit to gene expression data by Dolmetsch et al. [9]. (**A**) The model with antagonistic, oscillator-dependent regulation is able to perform band-pass activation (black line). No band-pass activation was observed for model versions without CaMKII or a calcium-independent CaMKII (overlapping blue lines). Red points mark the optimised values of $\overline{NFAT^*}$ for the following input periods: T_{fast} = 25 s, T_{med} = 60 s, T_{slow} = 500 s. (**B**) With the same parameter set, the model version exhibiting antagonistic, oscillator-dependent regulation indicates resemblance to NFAT gene expression data measured experimentally. The linearly scaled model data points, i.e. data points times β plus γ (black line), are displayed next to the raw data by Dolmetsch et al. [9] (black triangles). In contrast, the scaled truncated model versions fail in recreating the experimental measurements with respect to the initial peak in activity for fast oscillations (overlapping blue lines). Red points mark values of $\overline{NFAT^*}$ that were fitted to the gene expression data by Dolmetsch et al. For these outputs, we applied inputs that mimick experimental calcium oscillations (see Table 2). (For interpretation of the references to colour in this figure legend, the reader is referred to the web version of this article.)

We would like to note that we used square wave inputs with a constant active phase to produce the data in Fig. 3. This means that the average calcium concentration increases with increasing pulse frequency. The reason for this modelling choice was to stay as close as possible to the original experimental setup. However, applying square wave inputs with a constant average calcium concentration for different pulse frequencies (meaning that the active phase or pulse duration decreases with increasing frequency) to the same model, still allows for distinct band-pass activation (data not shown).

In its original form, the model includes antagonistic, oscillator-dependent regulation. We also tested alternative model versions, in which antagonistic calcium-dependent control was disrupted by either removing CaMKII entirely, i.e. deleting all reactions except for *N*3 to *N*4 and *N*9 to *N*10, or defining CaMKII to be independent of calcium by deleting *N*1 and *N*2 and setting $CaMKII^*$ to a constant level. In these cases, neither band-pass activation nor a resemblance to Dolmetsch et al.'s data could be achieved (Fig. 3, blue lines). This is a strong indication that antagonistic, oscillator-dependent regulation is a requirement for band-pass activation as defined here.

3.2. Minimal models for high-pass and band-pass activation

A model for high-pass activation was previously presented by Goldbeter et al. [33]. We adapted the model for this study. In particular, we included cooperative activation kinetics. The original model by Goldbeter et al. and our adapted version share a common topology, in which a calcium-dependent activator *A* fosters the generation of active decoder *P*, while a calcium-independent deactivator *D* controls *P*'s inactivation (Table 3). In the high-pass model with default parameter settings, fast calcium oscillations lead to an accumulation of *P* to an elevated level. This is caused by the input oscillations being so fast that *P* cannot be deactivated to its former levels during the trough of each oscillation period. In contrast, for slower calcium oscillations, *P* picks up the upstream oscillations and starts to oscillate itself, causing *P*'s concentration to stay below the previously mentioned elevated plateau for most of the time. Hence, the average activity $\overline{P}$ is larger for fast inputs and lower for slow inputs (Fig. 4).

Our observation that antagonistic, calcium-dependent regulation allows for band-pass activation (Section 3.1) in combination with insights on the dynamics of the high-pass model helped us to construct a minimal model for band-pass activation. In the resulting minimal model, the generation and degradation of active decoder *P* is controlled by two regulators, *A* and *D*, both of which are calcium-dependent (cf. Table 3 for a detailed description of the model). We set up the model such that *D* is more responsive to the calcium oscillation signal and that it can deactivate *P* faster than *A* can activate it. The following behaviour

Table 3
Structure and kinetics of the high-pass and band-pass model. In the high-pass model, competent activator *A* is generated by binding of calcium *Ca*. *A* is then able to activate the decoder *P*, while a deactivator *D* causes *P*'s inactivation. *D*'s concentration is fixed to 5000 nM by default, thus, only reactions v_{1-2} and v_{5-6} are part of the high-pass model. In contrast, in the band-pass model, *D*'s concentration is set variable, with competent *D* being generated by binding of *Ca*. For the band-pass model, reactions v_{1-6} apply. In the models, *Ca* is defined as a sine wave function as shown in Eq. (1).

Reactions			Kinetics
A_i	$\xrightarrow{Ca}$	A	$v_1 = \frac{k_{A1} \cdot A_i \cdot Ca^a}{K_A{}^a + Ca^a}$
A	$\rightarrow$	A_i	$v_2 = k_{A2} \cdot A$
D_i	$\xrightarrow{Ca}$	D	$v_3 = \frac{k_{D1} \cdot D_i \cdot Ca^d}{K_D{}^d + Ca^d}$
D	$\rightarrow$	D_i	$v_4 = k_{D2} \cdot D$
P_i	$\xrightarrow{A}$	P	$v_5 = \frac{k_{P1} \cdot P_i \cdot A^{P1}}{K_{P1}{}^{P1} + A^{P1}}$
P	$\xrightarrow{D}$	P_i	$v_6 = \frac{k_{P2} \cdot P \cdot D^{P2}}{K_{P2}{}^{P2} + D^{P2}}$

was obtained: For fast input oscillations, both regulators accumulate and reach elevated levels. Since *D* was defined to have a stronger effect on the conversion of the decoder, $\overline{P}$ is kept at low levels. When gradually slowing down the input oscillations, the more responsive *D* first starts to respond to the input's dynamics, causing it to decline from its elevated level. In contrast, the less responsive *A* remains closer to its elevated level for oscillations in an intermediate frequency range. In this range, *A* can compensate for its weaker control over *P*, as it is more abundant than *D*. As a result, $\overline{P}$ increases significantly. A further slowdown of the calcium input leads to *A* also starting to oscillate and to leave its elevated level. The previously observed concentration advantage is then lost and *D* becomes dominant once again, thus $\overline{P}$ declines (Fig. 5).

Furthermore, we tested whether the adapted version of the model by Goldbeter et al. could also support band-pass activation. In our optimisation runs, we were unable to find parameter settings with which this is achieved. In contrast, our minimal band-pass model was also able to exhibit high-pass activation (for more information please refer to the Supplementary material).

We would like to remark that, while we were working on this manuscript, we noticed in a conversation with our colleagues Aguilera et al. that they are studying the advantages and disadvantages of amplitude- and frequency-decoding in the light of robustness against changes in temperatures. In their study they use a model for decoding that has the same characteristics, e.g. structure and ability for band-pass activation, as our minimal band-pass activation model. Both models

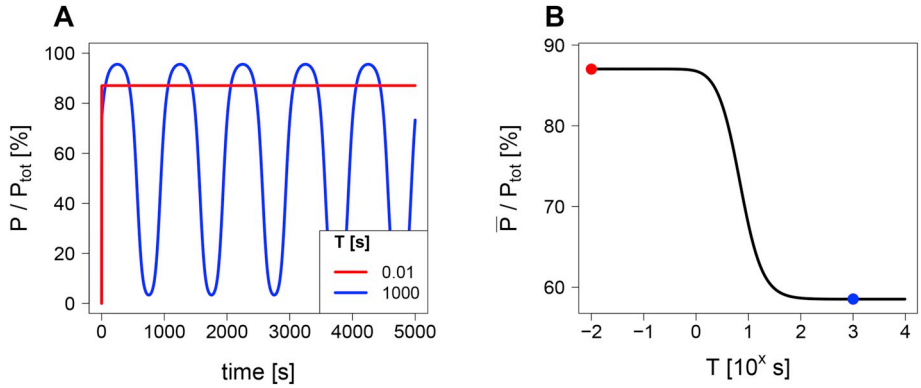

Fig. 4. Frequency-decoding in the high-pass model. (**A**) Fast calcium oscillations lead to an accumulation of active decoder *P*. A slowdown of the input dynamics results in *P* following the upstream oscillations. (**B**) Measurements of *P*'s average activity $\overline{P}$ confirm a significant drop upon stimulation with slower calcium oscillations. Colour-coded points refer to the time courses in the left panel. For information on the applied model parametrisation, please refer to the Supplementary material.

were developed independently. We would like to refer the interested reader to the article by Aguilera et al. [40].

3.3. The importance of cooperativity for frequency-decoding

As described in the introduction, a noticeable number of calcium-dependent proteins bind calcium ions or calmodulin-calcium complexes in a cooperative manner. This is accounted for in our frequency-decoder models by the implementation of several cooperative activation kinetics. Apart from cooperative binding of *Ca* to regulator species, *P* can also be regulated cooperatively by *A* and *D*.

We optimised high-pass and band-pass activation efficiencies, Eff_H and Eff_B (Eqs. (3) and (5)), for a number of different parametrisations of the cooperativity coefficients, yielding the high-pass and band-pass activation potentials, E_H and E_B (Eqs. (4) and (6)). For the maximisation of high-pass activation, rate and binding constants of the high-pass model were optimised. An increase in the cooperativity coefficient *a*, that describes the binding of calcium ions to the inactive activator form A_i, clearly results in an increase in E_H (Fig. 6 panel A and Fig. 7 panel A, black line). Additional increases in the cooperativity coefficients at the sites of *P*'s activation and deactivation causes E_H to grow even larger (Fig. 7 panel A, blue line).

For the maximisation of band-pass activation, rate and binding constants of the band-pass model were optimised. Pronounced band-pass activation was achieved, when cooperativities of both, the activating and deactivating branch, were increased at the same time (Fig. 6 panel B and Fig. 7 panel B, orange, black and grey lines). Increased cooperativities in only the activating or deactivating branch, did not result in an increased E_B. In fact, band-pass activation was disrupted, when enhancing either *a* or *d* alone (Fig. 7 panel B, red and blue lines). Thus, band-pass activation as modelled here, requires a balanced interplay between an activating and a deactivating force. As for the high-pass model, a concatenation of cooperative binding events leads to the largest observed values of E_B (Fig. 7 panel B, orange line).

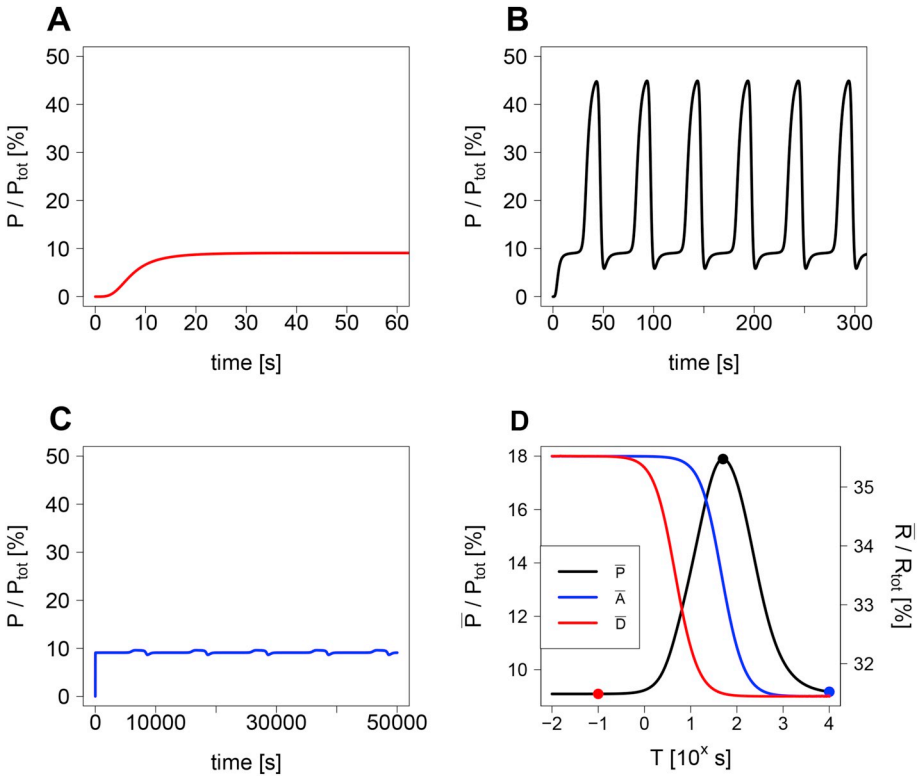

Fig. 5. Frequency-decoding in the band-pass model. The band-pass model was stimulated with very fast ($T = 0.1$ s; **A**), medium fast ($T = 50$ s; **B**) and slow ($T = 10{,}000$ s; **C**) sine waves. On average *P*'s concentration was highest for medium fast inputs, due to an on average higher abundance of *A* compared to *D*. Visualization of $\overline{P}$ revealed an optimal period length for *P*'s activation (**D**). Colour-coded points refer to the input periods used in the simulations presented in panels **A** to **C**. $\overline{R}$ refers to either $\overline{A}$ or $\overline{D}$. The applied model parameters can be found in the Supplementary material.

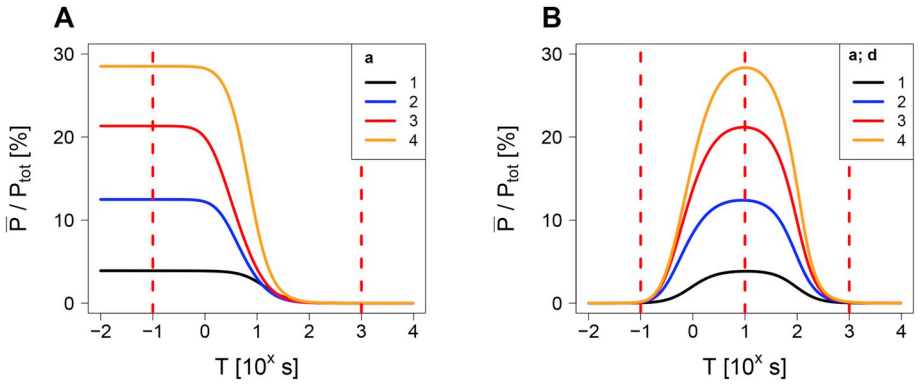

Fig. 6. Increases in cooperativity coefficients pronounce the distinctness in high-pass and band-pass activation. (**A**) Rate and binding constant parameters of the high-pass model were optimised in order to maximise the high-pass activation efficiency Eff_H. Clearly, increases in the cooperativity coefficient a result in a significant increase in the distinctness of high-pass activation. (**B**) Similarly, rate and binding constant parameters of the band-pass model were optimised in order to maximise the band-pass activation efficiency Eff_B. Increases in the cooperativity coefficients a and d cause an increase in the distinctness of band-pass activation. The minimal concentration of each curve was scaled to 0% to allow for a better comparison. Dashed red lines refer to the applied input period lengths T_{fast}, T_{med} and T_{slow}. All optimised parameter sets can be found in the Supplementary material. (For interpretation of the references to colour in this figure legend, the reader is referred to the web version of this article.)

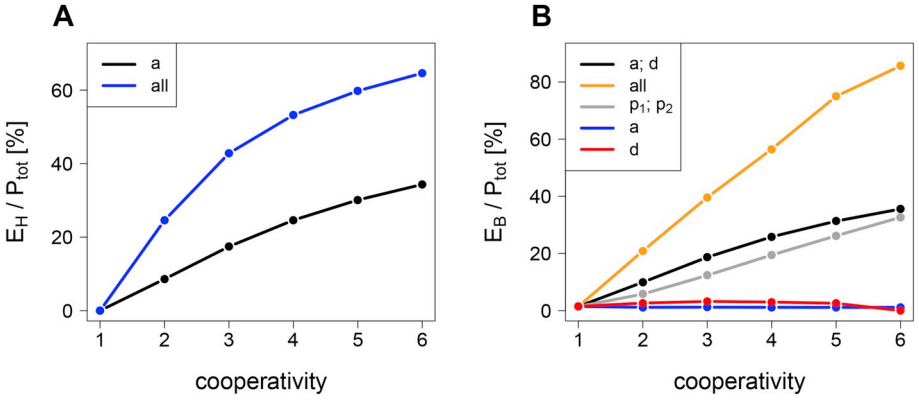

Fig. 7. Optimisation results for various parametrisations of cooperativity coefficients in the high-pass and band-pass model. Binding and rate constants of the high-pass and band-pass model were optimised in order to obtain high-pass and band-pass activation potentials, E_H and E_B, for different cooperativity coefficient parametrisations. (**A**) E_H clearly increases for increasing values of a (black line). A concatenation of cooperative events further elevates E_H (blue line). (**B**) E_B rises upon simultaneous increases in cooperativity coefficients of the activating and the deactivating model branch (orange, black and grey). Again a concatenation of cooperative events further elevates the activation potential (orange). Strengthening of either the activating or deactivating branch alone, does not lead to an increase in E_B (red and blue lines). The minimal concentration of each line was scaled to 0% to allow for a better comparison. For the optimisations, default values for T_{fast}, T_{med} and T_{slow} were employed. Optimised parameter sets can be found in the Supplementary material. (For interpretation of the references to colour in this figure legend, the reader is referred to the web version of this article.)

3.4. Parametric requirements for efficient frequency-decoding

We sought to investigate which parameter regions allow for efficient high- or band-pass activation. To this end, we employed a multi-start optimisation scheme for the optimisation of Eff_H and Eff_B. In particular, we examined optimisation results for a maximisation of Eff_H in the high-pass model for different parametrisations of a, and for a maximisation of Eff_B in the band-pass model for different parametrisations of a and d. A global optimum was approximated by running several thousands of optimisation runs per optimisation problem using the Nelder-Mead algorithm with different initial values of the optimisation parameters. The total concentration of each species and the cooperativities were fixed, all other parameter values were allowed to be changed by the optimisation.

We found that for all optimisation problems a substantial number of optimised parameter sets could induce objective values close to the overall best value found (quantitative information is given in the captions of Figs. 8 and 9). In order to assess parametric constraints in the best fits, we selected all parameter sets within a 2-nM-margin from the overall best objective value for particular optimisation problems and studied the parameter distributions in these best fits. All selected parameter sets allow for distinct high-pass or band-pass activation (in the Supplementary material, distributions of behaviours for the cooperativity values of $a = 4$ in the high-pass model and $a = d = 4$ in the band-pass model are presented).

In case of the high-pass model, binding constants are mostly distributed between 10^3 nM and 10^6 nM, well in the physiological range for enzymes [34]. Further, increases in the cooperativity a lead to a shift in the binding constant distributions towards lower values, most prominently in K_A's distribution (Fig. 8 panels E to G). The degradation rate k_{P2} is the most confined parameter, indicating a high sensitivity. Also the model's second degradation rate, k_{A2}, is severely confined for larger values of a (Fig. 8 panels B and D). In contrast, the corresponding production rates, k_{A1} and k_{P1}, show less constraints (Fig. 8 panels A and C). For all parameter sets capable of inducing efficient high-pass activation, k_{P2} was smaller than k_{P1}. However, we found that this relation was influenced by the model's initial value of D being fixed to a relatively high value of 5000 nM. In this case, the impact of the deactivator D on decoder inactivation has to be reduced to allow for high-pass activation. When decreasing the initial concentration of D, we could also find a few parameter sets leading to efficient high-pass activation with $k_{P2} > k_{P1}$ (for more information, please refer to the Supplementary material).

For the band-pass model, the parameter values of all binding constants are also distributed between 10^3 nM and 10^6 nM in the best fits. Again, a shift to lower values is observable for increasing cooperativity coefficients, especially for K_A's and K_D's distributions (Fig. 9 panels G to J). The degradation rates, k_{A2} and k_{D2}, were by far the most confined parameters, indicating a strong influence of these parameters on band-pass activation in the model (Fig. 9 panels B and D). Furthermore, all selected parameter sets capable of efficient band-pass activation exhibited k_{A2}-values smaller than the corresponding k_{D2}- and k_{P2}-values (Fig. 9 panels K and L).

3.5. Restricting parameter ranges in optimisations reveals how decoding degenerates for suboptimal parameter sets

In the last section, we showed that most parameter values in models

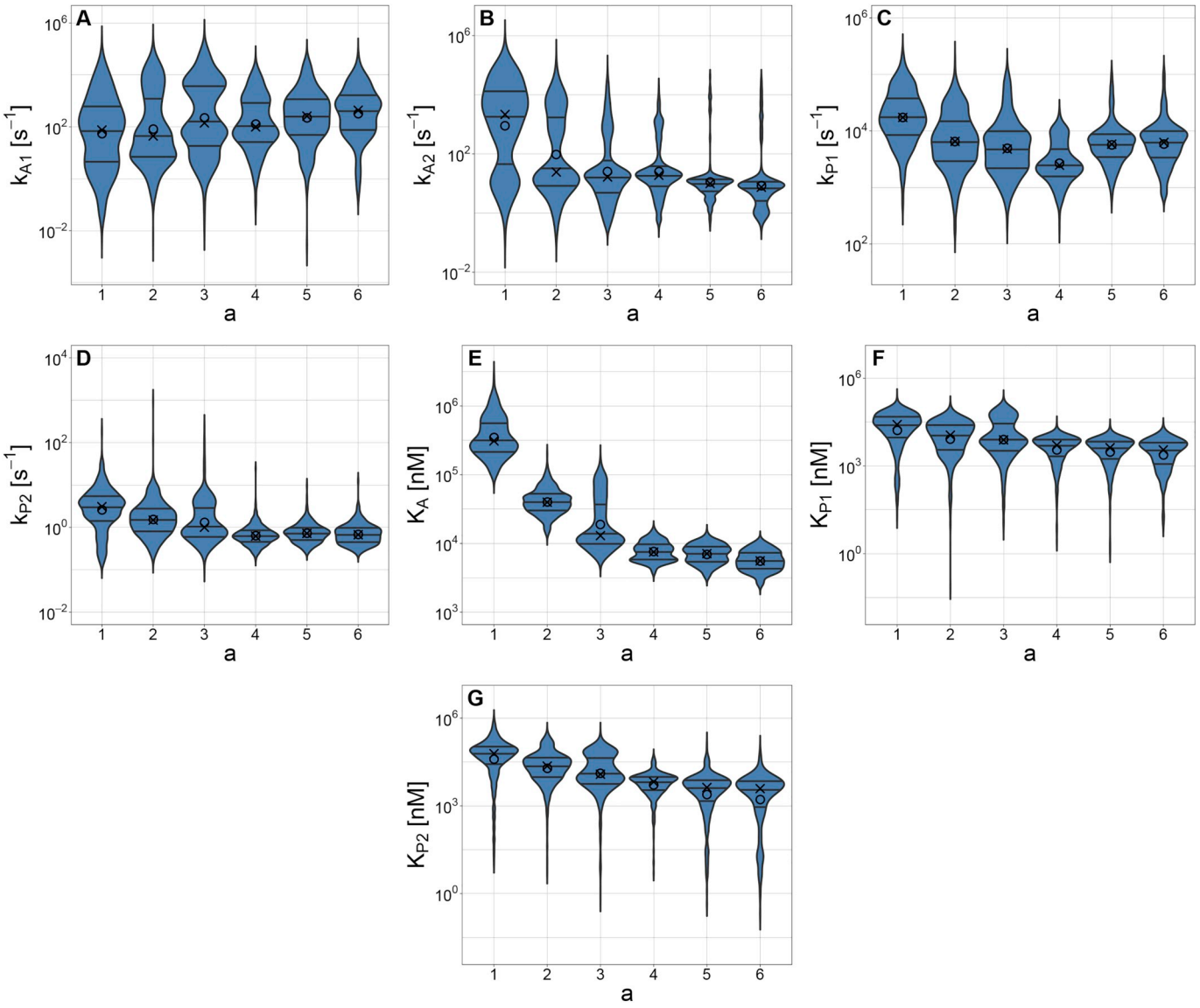

Fig. 8. Parameter distributions of parameter sets capable of efficient high-pass activation. Parameter sets leading to objective values within a 2-nM-margin to an overall best value were isolated per optimisation problem. Optimisations targeted a maximisation of the high-pass activation efficiency Eff_H for several parametrisations of the cooperativity coefficient a in the high-pass model (Table 3). Circles refer to the mean, crosses to the median of the parameter distributions. K_A's distributions indicates a decrease upon increases in a (**E**). The degradation rates k_{P2} and, for higher cooperativity values, also k_{A2} are the most confined parameters (**B** and **D**). For all analzyed cooperativity values, binding constants are mostly confined to a margin spanning from 10^3 nM to 10^6 nM (**E** to **G**). Absolute number of isolated parameter sets for $a = 1, 2, \ldots, 6$: 638, 982, 981, 483, 408, 344. Number of isolated parameter sets relative to the overall number of parameter sets for $a = 1, 2, \ldots, 6$: 13.13%, 50.51%, 52.43%, 65.27%, 29.96%, 44.73%. 2 nM relative to the leading objective value for $a = 1, 2, \ldots, 6$: 1.02%, 0.32%, 0.19%, 0.14%, 0.12%, 0.1%.

capable of efficient high-pass or band-pass activation are confined to specific intervals. Based on this, we wanted to investigate what effects stronger constraints on parameter values have on the models' frequency-decoding capabilities. We divided the model parameters into two groups, i.e. rate and binding constants. By increasing the lower parameter limit and/or decreasing the upper parameter limit, we performed constraint optimisation runs to examine the influence of the parameters on frequency-decoding.

In both cases, optimisation of high-pass activation in the high-pass model ($a = 4$) as well as optimisation of band-pass activation in the band-pass model ($a = d = 4$), a constriction of binding constants to values below 10^3 nM or above 10^5 nM results in a decrease in E_H and E_B, respectively (Fig. 10 panels A and B). These results are in accordance with optimal parameter value ranges found in Figs. 8 and 9 for cooperativities $a = 4$ and $a = d = 4$, respectively.

As for previous optimisations, we set up the algorithm to perform high-pass and band-pass activation at default period lengths, T_{fast}, T_{med} and T_{slow}. Severely lowering the upper rate constant limit, U_R, or raising the lower rate constant limit, L_R, causes the models to fail to decode frequencies at the default period lengths. In particular, a raise in L_R leads to accelerated systems with decoding shifted towards smaller period lengths T. While a lowering of U_R results in slower systems with decoding shifted towards larger values of T (Fig. 10 panels C to F).

4. Discussion

Frequency-decoding of calcium oscillations was reported for several proteins [4]. We defined two distinct variants of frequency-decoding, named high-pass and band-pass activation, that were observed experimentally. A protein performs high-pass activation, if it is strongly

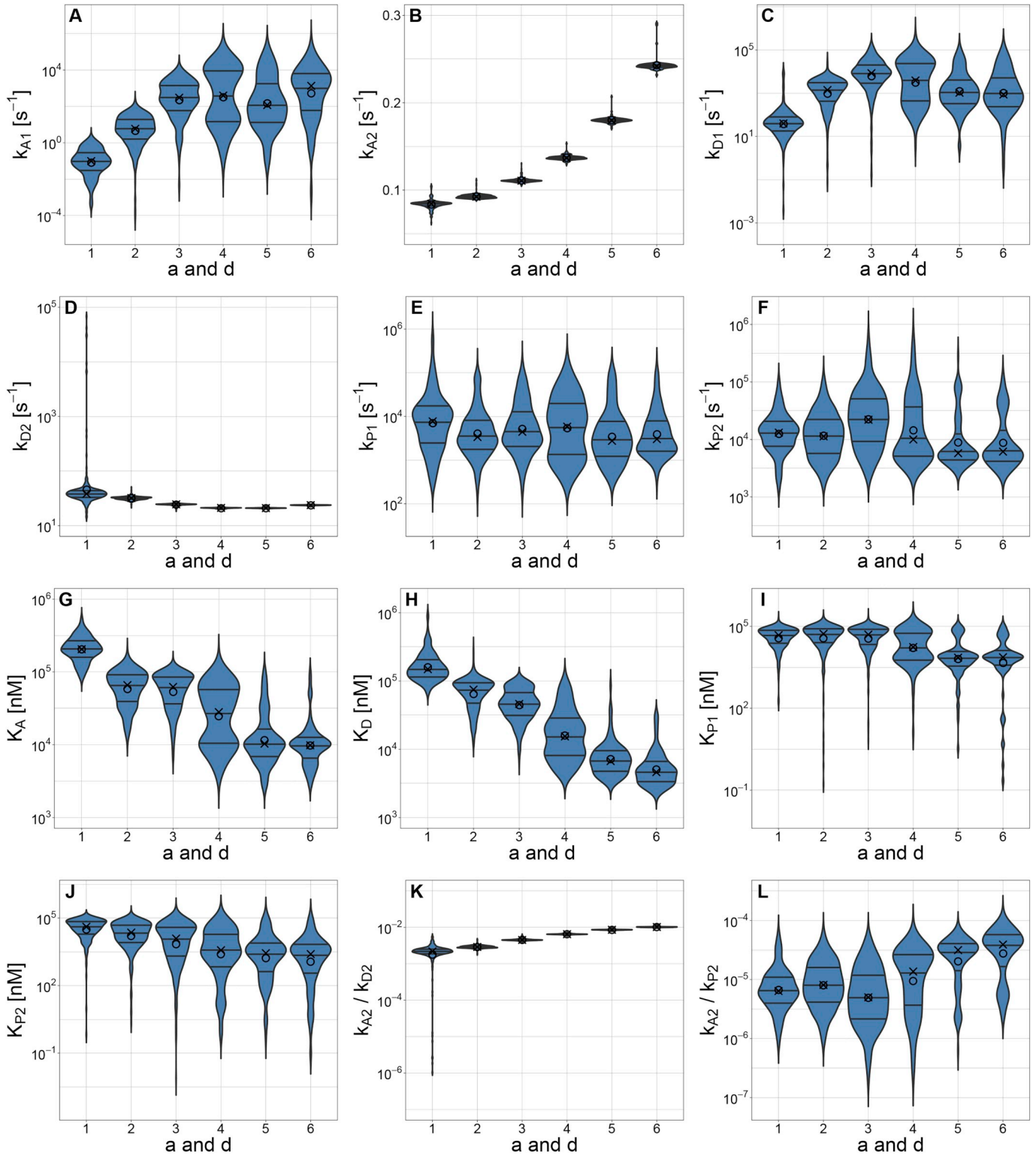

Fig. 9. Parameter distributions of parameter sets capable of efficient band-pass activation. Parameter sets leading to objective values within a 2-nM-margin of an overall best value were isolated per optimisation problem. Optimisations targeted a maximisation of the band-pass activation efficiency Eff_B for several parametrisations of the cooperativity coefficients a and d in the band-pass model. Circles refer to the mean, crosses to the median of the parameter distributions. The regulators' degradation rates, k_{A2} and k_{D2}, are the most confined parameters (**B** and **D**). For the binding constants, an optimal margin between 10^3 nM and 10^6 nM is recognisable. A drop in the binding constant distributions is visible upon increases in a and d. This is most apparent for the regulators' binding constants (**G** to **J**). Strikingly, A's degradation rate is always smaller than D's and P's in the isolated parameter sets (**K** and **L**). Absolute number of isolated parameter sets for a and d = 1, 2, …, 6: 254, 431, 416, 152, 121, 79. Number of isolated parameter sets relative to the overall number of parameter sets for a = 1, 2, …, 6: 3.12%, 5.88%, 6.28%, 1.88%, 0.76%, 0.28%. 2 nM relative to the leading objective value for a and d = 1, 2, …, 6: 1.04%, 0.33%, 0.19%, 0.14%, 0.12%, 0.11%.

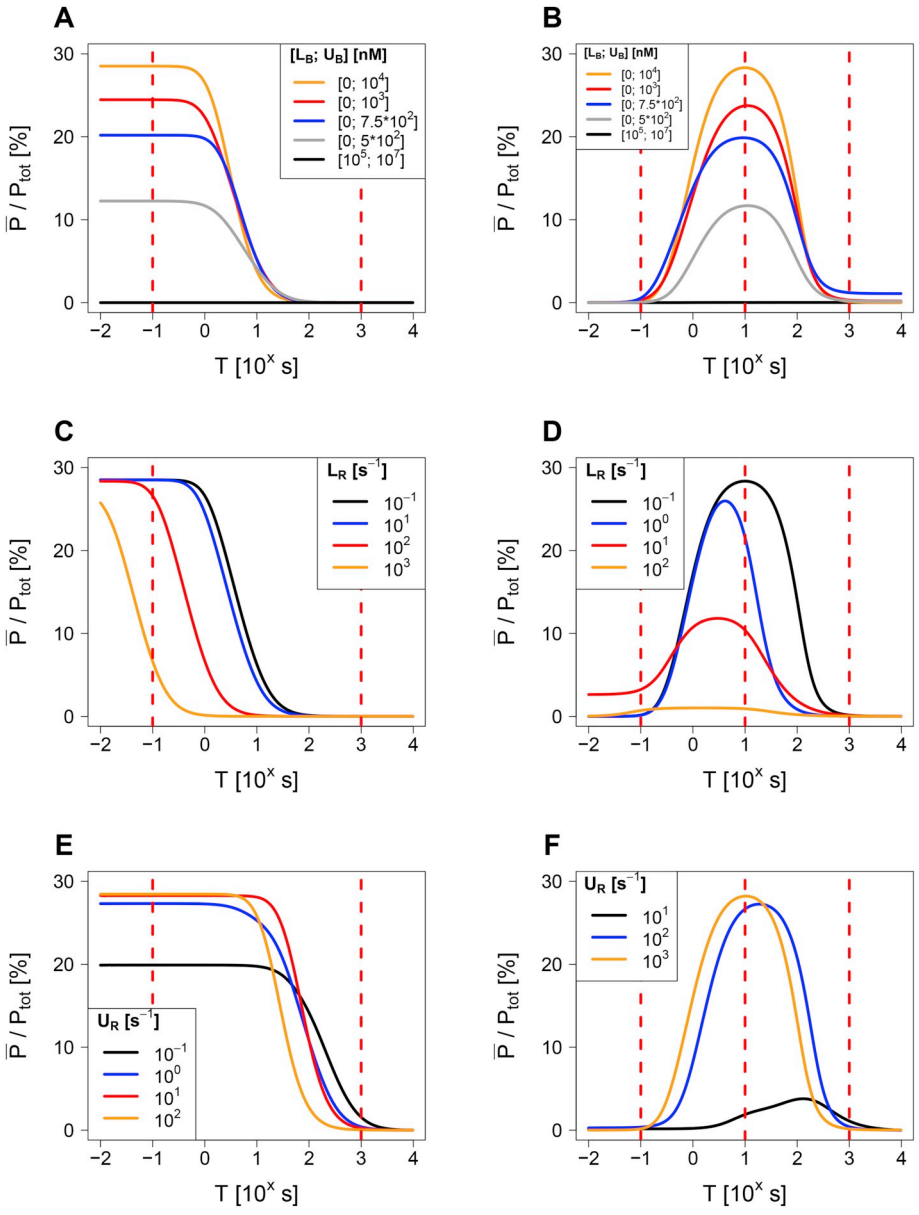

Fig. 10. Effect of constraint rate and binding constant parametrisation in high-pass and band-pass activation. Binding and rate constants were optimised in optimisation runs targeting either a maximisation of Eff_H in the high-pass model (**A**, **C** and **E**) or a maximisation of Eff_B in the band-pass model (**B**, **D** and **F**). In **A** and **B**, the models' binding constants were only allowed to vary in a margin spanning from L_B to U_B. In both instances, a constriction of binding constants to values outside of an optimal margin roughly spanning from 10^3 nM to 10^5 nM leads to a decline in E_H and E_B. In **C** to **F**, the models' rate constants were only allowed to vary in a margin spanning from either 0 to U_R or L_R to 10^5 s^{-1}. Severe constriction of rate constants results in models being unable to perform frequency-decoding over the desired bandwidths determined by the set period lengths T_{fast}, T_{med} and T_{slow}. Raising L_R causes an acceleration of the systems and a subsequent shift of decoding towards smaller values of T (**C** and **D**), whereas lowering U_R causes a slowdown and a subsequent shift of decoding towards larger values of T (**E** and **F**). The minimal concentration of each curve was scaled to 0% to allow for a better comparison. All optimised parameter sets can be found in the Supplementary material.

activated at fast oscillations and only weakly at slow oscillations, whereas proteins exhibiting band-pass activation feature an optimal frequency for their activation. Based on a presented optimisation scheme, we maximised the distinctness of both frequency-decoding modes in order to analyse the decoding capability of models as well as to quantify favourable parameter margins for efficient decoding given specific conditions.

With respect to the transcription factor NFAT, experimental studies suggest a band-pass activation mechanism for its gene expression activity [4,10]. By means of a model of NFAT activation in the cytosol, we could show that band-pass activation at experimentally observed frequencies was reproducible given an antagonistic, oscillator-driven regulation was implemented. Since NFAT's translocation to the nucleus is actually activated by calcium-dependent calcineurin [14,31] and inhibited by calcium-dependent CaMKII [17,18], we assume antagonistic, calcium-dependent regulation to be also a requirement for NFAT's band-pass activation in real cells.

On the basis of a model by Goldbeter et al. [33] and results gained with the NFAT model, we constructed minimal models for high-pass and band-pass activation. While in the high-pass model only the activation of a decoder protein is calcium-dependent, in the band-pass model deactivation is also dependent on calcium. It was found that the band-pass model can also work as a high-pass decoder given a suitable parameter set, whereas the high-pass model, lacking the necessary antagonistic, oscillator-dependent regulation, cannot achieve band-pass activation (presented in the Supplementary material). Therefore, we once more conclude that antagonistic, oscillator-dependent regulation is a requirement for more complex decoding capabilities.

We demonstrated, how increases in the cooperativity strength leads to an increase in the models' frequency-decoding potentials. With respect to the band-pass activation model, only a balanced increase in the cooperativites of the activating and deactivating branch raises the band-pass potential E_B. Increasing only the cooperativity in one branch does not benefit the distinctness of band-pass activation. The need for a balance of forces in the band-pass model underlines the premise of antagonistic, oscillator-dependent regulation for band-pass activation. In addition, we found a concatenation of cooperative activation events to be most powerful in raising high-pass as well as band-pass decoding potentials. It might be possible that concatenative effects play a role in activation mechanisms employing calmodulin as an intermediary. Thus, cooperative activation of calmodulin by binding of calcium ions [35] followed by cooperative activation of a calmodulin substrate by binding

of calmodulin-calcium complexes [22,36] could result in a significantly increased frequency-decoding capability. Generally, we believe that cooperative activation, as commonly observed among decoders of calcium oscillation frequency [22–24], might have been emerged in the course of evolution to pronounce frequency-selective behaviour.

In-depth analyses of parameter sets capable of efficient high-pass or band-pass activation for different parametrisations of cooperativity coefficients yielded the identification of parametric constraints necessary to perform distinct frequency-decoding. Particularly, binding constant parameters were confined to a margin between 10^3 nM and 10^5 nM, well in the range of comparable parameters in physiology [34]. Furthermore, efficient band-pass activation in the band-pass model required k_{A2} values lower than the corresponding k_{D2} and k_{P2} values. The resulting time scale separation in the band-pass model is in line with our initial guess for the generation of band-pass activation, as described in the results.

In addition, we analysed the effect of unfavourable parametrisation constraints in optimisations of high-pass and band-pass efficiencies. For both, a parametrisation of binding constants outside of the described optimal interval resulted in decreased high-pass and band-pass potentials. The models were not able to reproduce frequency-decoding as efficiently as before. When constricting rate constants to larger values, the system was accelerated, causing it to shift its frequency-decoding towards higher frequencies. The opposite was observed upon constricting the rate constants to smaller values. Thus, a severe constriction of rate constants leads to systems failing to exhibit distinct frequency-decoding over a desired bandwidth, as defined by T_{fast}, T_{med} and T_{slow}. As a conclusion, rate constant parametrisation is directly dependent on the targeted bandwidth for frequency-decoding. We believe, it is likely that bandwidths usable in frequency-decoding are constrained by physiological boundaries in cells. On the one hand very slow bandwidths cannot be unlocked, since systems must not be too slow for signal processing. After all decoding is bound to occur on a reasonable time scale. On the other hand very fast bandwidths remain out of range, since a system fast enough for decoding, would likely require excessive amounts of energy.

Although band-pass activation driven by calcium oscillations has not been reported for other proteins except for NFAT, we expect further proteins to indicate a similar behaviour. Antagonistic, calcium-dependent control was found to be a major requirement for the existence of band-pass activation and indeed several reports identified calcium-dependent kinase-phosphatase couples as common regulators of signalling pathways: Runyan et al. showed how calcineurin and CaMKII modulate working memory [37], Wen et al. demonstrated how calcineurin and CaMKII switch growth cone guidance control in axons [38] and Nasipak et al. found PKC and calcineurin to have opposing roles in skeletal muscle differentiation [39]. This does not mean that band-pass activation is definitely present in these pathways, yet it exemplifies that antagonistic, calcium-dependent regulation is a common motif in cells. Compared to high-pass activation, band-pass activation is much preciser in regulating the activities of several calcium-dependent proteins in parallel. Particular bandwidths of calcium oscillations could be associated with activating only a certain subset of proteins, while entirely different subsets of proteins could be activated at faster and slower bandwidths. Especially in terms of the control of proteins exerting opposing cell functions like proliferation and apoptosis or having a high toll in terms of energy consumption, a tightly controlled, differential activation mechanism would offer considerable advantages.

Finally, we would like to note that our workflow is not limited to the study of calcium frequency-decoding but can also be very useful for the testing for other model characteristics in signalling systems.

Declaration of interest

None.

Acknowledgements

AS and JP would like to thank the Center for Modelling and Simulation in the Biosciences (BIOMS) for financial support. AS and JP would also like to thank Jonas Förster, Michael Gabel, Frederik Graw, Ursula Kummer, Sarah Kaspar, Irina Surovtsova and Martin Zauser for fruitful discussions.

Appendix A. Supplementary data

Supplementary data to this article can be found online at https://doi.org/10.1016/j.bpc.2018.10.005.

References

[1] Michael J. Berridge, Martin D. Bootman, Peter Lipp, Calcium - a life and death signal, Nature 395 (6703) (1998) 645, https://doi.org/10.1038/27094.
[2] Niall M. Woods, K.S. Roy Cuthbertson, Peter H. Cobbold, Repetitive transient rises in cytoplasmic free calcium in hormone-stimulated hepatocytes, Nature 319 (6054) (1986) 600–602, https://doi.org/10.1038/319600a0.
[3] C. Jane Dixon, Niall M. Woods, K.S. Roy Cuthbertson, Peter H. Cobbold, Evidence for two Ca^{2+} −mobilizing purinoceptors on rat hepatocytes, Biochem. J. 269 (2) (1990) 499–502.
[4] Erik Smedler, Per Uhlén, Frequency decoding of calcium oscillations, Biochim. Biophys. Acta Gen. Subj. 1840 (3) (2014) 964–969, https://doi.org/10.1016/j.bbagen.2013.11.015.
[5] Ann Zahle Larsen, Lars Folke Olsen, Ursula Kummer, On the encoding and decoding of calcium signals in hepatocytes, Biophys. Chem. 107 (1) (2004) 83–99, https://doi.org/10.1016/j.bpc.2003.08.010.
[6] Paul De Koninck, Howard Schulman, Sensitivity of CaM kinase II to the frequency of Ca^{2+} oscillations, Science 279 (5348) (1998) 227–230, https://doi.org/10.1126/science.279.5348.227.
[7] Elena Oancea, Tobias Meyer, Protein kinase C as a molecular machine for decoding calcium and diacylglycerol signals, Cell 95 (3) (1998) 307–318, https://doi.org/10.1016/S0092-8674(00)81763-8.
[8] P. Tompa, R. Töth-Boconádi, P. Friedrich, Frequency decoding of fast calcium oscillations by calpain, Cell Calcium 29 (3) (2001) 161–170, https://doi.org/10.1054/ceca.2000.0179.
[9] Ricardo E. Dolmetsch, Xu Keli, Richard S. Lewis, Calcium oscillations increase the efficiency and specificity of gene expression, Nature 392 (6679) (1998) 933, https://doi.org/10.1038/31960.
[10] Wen Li, Juan Llopis, Michael Whitney, Gregor Zlokarnik, Roger Y. Tsien, Cell-permeant caged InsP3 ester shows that Ca^{2+} spike frequency can optimize gene expression, Nature 392 (6679) (1998) 936–941, https://doi.org/10.1038/31965.
[11] Michael R. Tadross, Ivy E. Dick, David T. Yue, Mechanism of local and global Ca^{2+} sensing by calmodulin in complex with a Ca^{2+} channel, Cell 133 (7) (2008) 1228–1240, https://doi.org/10.1016/j.cell.2008.05.025.
[12] Taichiro Tomida, Kenzo Hirose, Azusa Takizawa, Futoshi Shibasaki, Masamitsu Iino, NFAT functions as a working memory of Ca^{2+} signals in decoding Ca^{2+} oscillation, EMBO J. 22 (15) (2003) 3825–3832, https://doi.org/10.1093/emboj/cdg381.
[13] Per Uhlén, Peter M. Burch, Christina Ivins Zito, Manuel Estrada, Barbara E. Ehrlich, Anton M. Bennett, Gain-of-function/Noonan syndrome SHP-2/Ptpn11 mutants enhance calcium oscillations and impair NFAT signaling, Proc. Natl. Acad. Sci. U. S. A. 103 (7) (2006) 2160–2165, https://doi.org/10.1073/pnas.0510876103.
[14] Matilde Colella, Francesca Grisan, Valerie Robert, Jay D. Turner, Andrew P. Thomas, Tullio Pozzan, Ca^{2+} oscillation frequency decoding in cardiac cell hypertrophy: role of calcineurin/NFAT as Ca^{2+} signal integrators, Proc. Natl. Acad. Sci. 105 (8) (2008) 2859–2864, https://doi.org/10.1073/pnas.0712316105.
[15] Chan R. Beals, Colleen M. Sheridan, Christoph W. Turck, Phyllis Gardner, Gerald R. Crabtree, Nuclear export of NF-ATc enhanced by glycogen synthase kinase-3, Science 275 (5308) (1997) 1930–1933, https://doi.org/10.1126/science.275.5308.1930.
[16] Cynthia M. Porter, Michael A. Havens, Neil A. Clipstone, Identification of amino acid residues and protein kinases involved in the regulation of NFATc subcellular localization, J. Biol. Chem. 275 (5) (2000) 3543–3551, https://doi.org/10.1074/JBC.275.5.3543.
[17] Scott M. MacDonnell, Jutta Weisser-Thomas, Hajime Kubo, Marie Hanscome, Qinghang Liu, Naser Jaleel, Remus Berretta, Xiongwen Chen, Joan H. Brown, Abdel-Karim Sabri, et al., CaMKII negatively regulates calcineurin-NFAT signaling in cardiac myocytes, Circ. Res. 105 (4) (2009) 316–325, https://doi.org/10.1161/CIRCRESAHA.109.194035.
[18] Yoshiaki Hashimoto, Marita M. King, Thomas R. Soderling, Regulatory interactions of calmodulin-binding proteins: phosphorylation of calcineurin by autophosphorylated Ca^{2+}/calmodulindependent protein kinase II, Proc. Natl. Acad. Sci. 85 (18) (1988) 7001–7005.
[19] Y. Hashimoto, T.R. Soderling, Regulation of calcineurin by phosphorylation. Identification of the regulatory site phosphorylated by Ca^{2+}/calmodulin-dependent protein kinase II and protein kinase C, J. Biol. Chem. 264 (28) (1989) 16524–16529.
[20] Nobuaki Hama, Fotini Paliogianni, Barri J. Fessler, Dimitrios T. Boumpas, Calcium/

calmodulindependent protein kinase II downregulates both calcineurin and protein kinase C-mediated pathways for cytokine gene transcription in human T cells, J. Exp. Med. 181 (3) (1995) 1217–1222.
[21] Shozo Iida, James D. Potter, Calcium binding to calmodulin. Cooperativity of the calcium-binding sites, J. Biochem. 99 (6) (1986) 1765–1772.
[22] Nicholas J. Carruthers, Paul M. Stemmer, Methionine oxidation in the calmodulin-binding domain of calcineurin disrupts calmodulin binding and calcineurin activation, Biochemistry 47 (10) (2008) 3085–3095, https://doi.org/10.1021/bi702044x.
[23] Julia M. Shifman, Mee H. Choi, Stefan Mihalas, Stephen L. Mayo, Mary B. Kennedy, Ca^{2+}/calmodulin-dependent protein kinase II (CaMKII) is activated by calmodulin with two bound calciums, Proc. Natl. Acad. Sci. 103 (38) (2006) 13968–13973, https://doi.org/10.1073/pnas.0606433103.
[24] Susy C. Kohout, Senena Corbalán-García, Alejandro Torrecillas, Juan C. Goméz-Fernandéz, Joseph J. Falke, C2 domains of protein kinase C isoforms α, β, and γ: activation parameters and calcium stoichiometries of the membrane-bound state, Biochemistry 41 (38) (2002) 11411–11424, https://doi.org/10.1021/bi026041k.
[25] C. Jane Dixon, Peter H. Cobbold, Anne K. Green, Actions of ADP, but not ATP, on cytosolic free Ca^{2+} in single rat hepatocytes mimicked by 2-methylthioATP, Br. J. Pharmacol. 116 (3) (1995) 1979–1984, https://doi.org/10.1111/j.1476- 5381.1995.tb16401.x.
[26] R Core Team, R: a language and environment for statistical computing, R Foundation for Statistical Computing. Vienna, Austria, 2017.
[27] Karline Soetaert, Thomas Petzoldt, R. Woodrow Setzer, Solving differential equations in R: package deSolve, J. Stat. Softw. 33 (9) (2010) 1–25 ISSN: 1548-7660 https://doi.org/10.1007/978-3-642-28070-2 http://www.jstatsoft.org/v33/i09.
[28] Linda Petzold, Automatic selection of methods for solving stiff and nonstiff systems of ordinary differential equations, SIAM J. Sci. Stat. Comput. 4 (1) (1983) 136–148, https://doi.org/10.1137/0904010.
[29] John A. Nelder, Roger Mead, A simplex method for function minimization, Comput. J. 7 (4) (1965) 308–313, https://doi.org/10.1093/comjnl/7.4.308.
[30] Gerald R. Crabtree, Stuart L. Schreiber, SnapShot: Ca^{2+} − calcineurin-NFAT signaling, Cell 138 (1) (2009) 210, https://doi.org/10.1016/j.cell.2009.06.026.
[31] Frank Rusnak, Pamela Mertz, Calcineurin: form and function, Physiol. Rev. 80 (4) (2000) 1483–1521, https://doi.org/10.1152/physrev.2000.80.4.1483.
[32] Geneviève Dupont, Gérald Houart, Paul De Koninck, Sensitivity of CaM kinase II to the frequency of Ca^{2+} oscillations: a simple model, Cell Calcium 34 (6) (2003) 485–497, https://doi.org/10.1016/S0143-4160(03)00152-0.
[33] Albert Goldbeter, Geneviève Dupont, Michael J. Berridge, Minimal model for signal-induced Ca^{2+} oscillations and for their frequency encoding through protein phosphorylation, Proc. Natl. Acad. Sci. 87 (4) (1990) 1461–1465, https://doi.org/10.1073/pnas.87.4.1461.
[34] Arren Bar-Even, Elad Noor, Yonatan Savir, Wolfram Liebermeister, Dan Davidi, Dan S. Tawfik, Ron Milo, The moderately efficient enzyme: evolutionary and physicochemical trends shaping enzyme parameters, Biochemistry 50 (21) (2011) 4402–4410, https://doi.org/10.1021/bi2002289.
[35] J.F. Maune, C.B. Klee, K. Beckingham, Ca^{2+} binding and conformational change in two series of point mutations to the individual Ca(2+)-binding sites of calmodulin, J. Biol. Chem. 267 (8) (1992) 5286–5295.
[36] Luke H. Chao, Patricia Pellicena, Sebastian Deindl, Lauren A. Barclay, Howard Schulman, John Kuriyan, Intersubunit capture of regulatory segments is a component of cooperative CaMKII activation, Nat. Struct. Mol. Biol. 17 (3) (2010) 264, https://doi.org/10.1038/nsmb.1751.
[37] Jason D. Runyan, Anthony N. Moore, Pramod K. Dash, A role for prefrontal calcium-sensitive protein phosphatase and kinase activities in working memory, Learn. Mem. 12 (2) (2005) 103–110, https://doi.org/10.1523/jneurosci.4880-03.2004.
[38] Zhexing Wen, Carmine Guirland, Guo Ming, James Q. Zheng, A CaMKII/calcineurin switch controls the direction of Ca^{2+} − dependent growth cone guidance, Neuron 43 (6) (2004) 835–846, https://doi.org/10.1016/j.neuron.2004.08.037.
[39] Brian T. Nasipak, Teresita Padilla-Benavides, Karin M. Green, John D. Leszyk, Wenjie Mao, Silvana Konda, Saïd Sif, Scott A. Shaffer, Yasuyuki Ohkawa, Anthony N. Imbalzano, Opposing calcium-dependent signalling pathways control skeletal muscle differentiation by regulating a chromatin remodelling enzyme, Nat. Commun. 6 (2015), https://doi.org/10.1038/ncomms8441.
[40] L. Aguilera, F.T. Bergmann, G. Dalmasso, S. Elmas, T. Elsässer, R. Großeholz, P. Holzheu, P. Kalra, U. Kummer, S. Sahle, N. Veith, Robustness of frequency vs. amplitude coding of calcium oscillations during changing temperatures, Biophysical Chemistry (2018), https://doi.org/10.1016/j.bpc.2018.11.003 (in press).